Electrochimica Acta 392 (2021) 138978

Contents lists available at ScienceDirect

Electrochimica Acta

journal homepage: www.elsevier.com/locate/electacta

Improved $Li_4Ti_5O_{12}$ electrodes by modified current collector surface

Christina Toigo[a,1,*], Martin Frankenberger[b], Nicolas Billot[c], Claudia Pscherer[d], Benedikt Stumper[c], Fabian Distelrath[d], Jonathan Schubert[b], Karl-Heinz Pettinger[b], Catia Arbizzani[a,1]

[a] Department of Chemistry "Giacomo Ciamician", Alma Mater Studiorum Universitá di Bologna, Bologna 40126, Italy
[b] Technology Center for Energy, University of Applied Sciences Landshut, Ruhstorf 94099, Germany
[c] Institute for Machine Tools and Industrial Management, Technical University of Munich, Garching 85748, Germany
[d] Carl Schlenk AG, Roth 91154, Germany

ARTICLE INFO

Article history:
Received 4 May 2021
Revised 10 July 2021
Accepted 19 July 2021
Available online 28 July 2021

Keywords:
Lithium-ion battery
Current collector
Lithium titanium oxide
LTO
Surface modification
Electrochemical impedance spectroscopy
Copper dendrites

ABSTRACT

A copper current collector is treated by electrolytic deposition of copper dendrites at the surface of the foil. This treatment results in a more structured surface leading to an improved contact between the electrode materials and the current collector. The contact to the electrode material particles of different sizes is investigated. Active materials of submicron size exhibit a drastically reduced internal resistance and a clearly improved C-rate capability. BET surface area measurement and calculation of roughness factor resulted in the finding of dendritic copper foil to provide an 8-fold larger surface area compared to the untreated foil. A comprehensive electrochemical impedance spectroscopy study is conducted for elucidation of electrochemical utilisation of the surface area increase. As a result, both fitting parameters for capacitance and surface resistance correspond to a similar normalization shift, indicating a clear improvement in the electro-active interface area.

1. Introduction

The optimization of lithium-ion batteries (LIB) is a very challenging task, given that each battery component needs to be carefully evaluated with regard to its way of working and an in-depth-understanding of optimization possibilities has to be generated. Our group has already evaluated the effect of lamination and the separator-electrode interphase [1,2] as well as electrode formulation with different binders [3,4]. Graphite is the ancestor of anode materials for LIBs, and up to now is the most used one for its good cycling performance. However, the solid electrolyte interphase (SEI) that is formed at the graphite/electrolyte interphase due to the electrolyte reactivity, can break and reform during repeated charge and discharge cycles [5]. Another possible anode material under investigation is silicon. By now, its commercialization is hindered by a massive volume expansion during cycling, although a proper combination of different strategies could enable high performing anodes based on silicon in the near future [6]. This work focuses on spinel $Li_4Ti_5O_{12}$ (LTO) that is an attractive alternative to graphite. It displays high cycling stability, fast kinetics and high rate capability. Its relatively high lithium insertion voltage of 1.55 V vs. Li/Li^+ avoids the electrochemical formation of a SEI from ethylene carbonate reduction [7,8]. In contrast to the mentioned advantages, LTO has scarce electrical conductivity and low Li-ion diffusion coefficient [8,9]. A number of different approaches has been attempted to overcome these drawbacks. Chou et al. have synthesized LTO nanomaterials with a high surface area to improve rate capability [7]. Carvalho et al. showed that the use of mild acids as pH-modifier and different polysaccharide binders affect LTO electrode morphology, adhesion and electrochemical properties [5]. Many other binders have been evaluated for their usability in combination with LTO in recent years, e.g. sodium alginate [3,4,6,7], carboxymethyl cellulose (CMC) [8], acrylic binder LA132 [9], PEG-based binder [10] or bio-derivative rosin [11].

Another promising approach to ameliorate LTO performance is the modification of the current collector in such a way that an improved contact with the active material is established and the overall resistance is significantly reduced. Different ways of modification have been under investigation, e.g. a thin layer of graphene applied on the surface of the Cu foil [12], carbon-coating on aluminium current collector [13], a laser structuring with various types of dot patterns [14], laser-assisted processing to the active

* Corresponding author.
E-mail address: christina.toigo2@unibo.it (C. Toigo).
[1] ISE Member

https://doi.org/10.1016/j.electacta.2021.138978

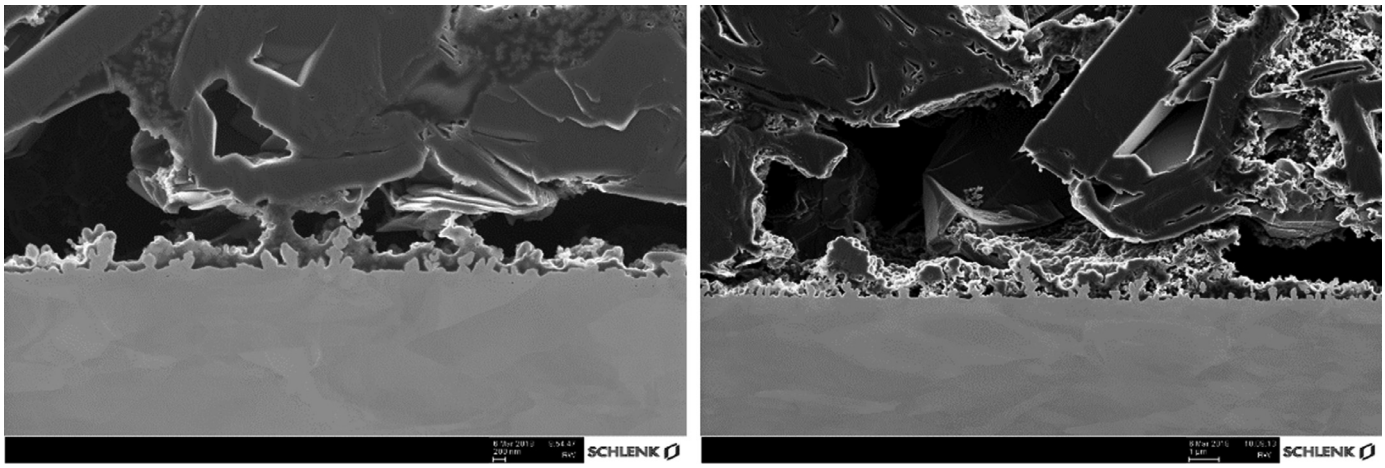

Fig. 1. SEM of dendritic foil covered with graphite particles.

material itself [15], synthetization of a compact oxide layer upon aluminium current collector [16], different surface morphologies of aluminium current collector [17] and so-called laser-induced periodic surface structures on steel and copper surfaces [18].

One type of modification derived from printed circuit board technology is the so-called nodular treatment. This treatment was established in the 1960s for enhancing the bonding strength of copper foil versus substrates used for printed circuit boards. The goal is to form interlocking structures on the copper surface for the epoxy resin. This is achieved by electrolytic deposition of copper dendrites onto the surface of the foil.

Here we report the effect of a galvanically structured copper current collector foil (SeCu58 with treatment) on the performance of LTO electrodes in comparison with a non-treated copper foil (SeCu58 blanc). The recipes' frame parameters (10% of conducting additives, 7% of binder, low loading of 0.5 mAh/cm², viscosity below 2000 mPa s) have been adopted to the question of whether an improvement in general can be achieved. So it is likely to minimize possible external influence factors like a limitation by electrical conductivity within the electrode coating or a limitation by Li-ion-diffusion.

2. Experimental

The galvanic structuring of the current collector Cu foil was achieved by a reel-to-reel plating line consisting of an electrolytic degreasing bath, an acidic activation bath containing diluted sulphuric acid (5 wt-%), a deposition tank and a chromate passivation with intermediate rinsing steps. The copper deposition was done using an acidic copper-sulphate based electrolyte and applying pulsed current at an average of 0.06 A/cm² for 29 s. After wet processing the substrate was dried in-line in a hot air oven.

LTO electrode formulation consisted of spherical $Li_4Ti_5O_{12}$ (83 wt-%, GN-LTO-1, GelonLIB, particle size D_{10} 0.1–0.5 μm, D_{50} 0.7–1.6 μm, tap density >= 0.65 g/cm³, specific surface area <= 16.0 m²/g), conductive carbon (10 wt-%, Super C65, Imerys) and polyvinylidene difluoride (PVDF, 7 wt-%, Solef 5130, Solvay) in a high-speed dissolver. Graphite electrodes were prepared by mixing 93 wt-% of graphite (MAGE3, D_{50} 22.8 μm, Hitachi Chemical), 1.33 wt-% CMC (Sunrose-MAC200 HC, NPI Chem), 2.67 wt-% SBR (SBR BM 451B, ZEON), 2 wt-% carbon black (Super C65, Imerys) and 1 wt-% conducting additive graphite (SFG6L, Imerys) in a planetary mixer.

Both graphite and LTO electrodes were casted in a roll-to-roll process coating machine on a standard Cu foil as well as on a galvanically structured Cu foil. The slurry was dried in-line in a four-step drying tunnel at a temperature range of 90 °C – 110 °C – 130 °C – 150 °C. The average loading of the as-prepared LTO anodes was 0.35 mAh/cm², compared to 2.1 mAh/cm² for the graphite anodes, which is close to the standard capacity of 2.4 to 2.5 mAh/cm² [19,20] used to evaluate mass transport phenomena. The mass loading of LTO anodes was based on a scientific approach to eliminate limitations of mass transport which is known to affect C-rate capability. Least possible limitation of mass transport requires a low coating thickness, whereas least possible electronic limitation needs a high amount of Super C as conducting agent. Both of these steps are not standardly integrated in slurry and electrode preparation.

Three electrode cell preparation was made as follows:

The LTO electrodes were punched into circular samples with a handheld punch (Nogamigiken Co., Ltd., Tokyo, Japan) with a size of 10 mm in diameter and dried in a drying chamber at 110 °C for 12 h under vacuum (Binder, APT.lineTM VDL 115 vacuum drying chamber with microprocessor-programme controller).

Lithium counter electrode disks (12 mm) were cut from elemental lithium. A lithium disk was placed on the stamp located in the cell (see Fig. 1 in appendix). Two 12 mm separator disks (glass microfiber filter, VWR) were placed on the lithium electrode. Additionally, lithium was punched with the smallest stamp of the half-cell components, which was used as reference electrode. The separators were filled with 100 µL of the electrolyte LP 572 (1 M $LiPF_6$ in EC/EMC 3/7 plus 2% VC). The LTO electrode with a diameter of 10 mm, was placed on the separator. At the upper opening, a separator (10 mm diameter) was placed and wetted with 40 µL LP 572. The lithium reference was placed on the separator and fixed with a sealed stamp and a screw cap. For all measurements three cells were assembled with a similar weight loading of the LTO working electrodes.

A Zeiss Auriga 40 FIB/SEM electron microscope was used to take micrographs and the colour figures were prepared from a FIB/SEM tomography using an energy selective backscatter detector (EsB). The stack of EsB images was then segmented and processed with the image processing software Dragonfly 4.1 to create the coloured images and also a 3D tomography. A self-constructed pull-off test bench was selected in order to measure the adhesion and cohesion of the anodes. The vertical movement to approach the sample to be investigated was carried out by a linear axis (CKK-145-NN-1) manufactured by Bosch Rexroth AG (Lohr am Main, Germany) and the force measurement was performed by 2.0 kN load cell (F2210) with a sampling rate of 5000 Hz from Tecsis GmbH (Offenbach, Germany). For the adhesion measurements, round samples were punched out with a handheld punch (Ø 15 mm), placed between

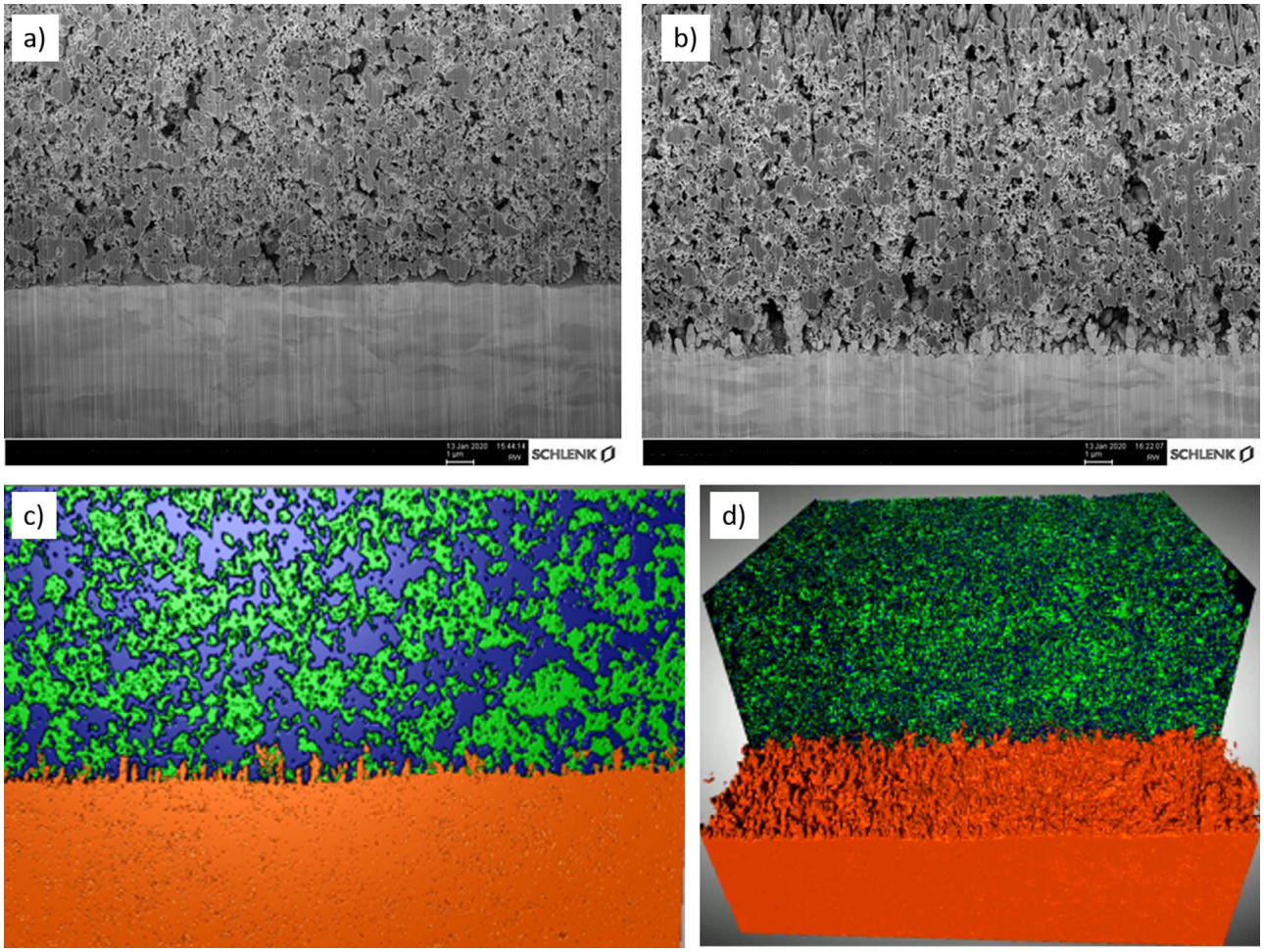

Fig. 2. SEM images of untreated (a) and dendritic (b-d) copper foil. Colour map for false-colour images c) and d): orange = copper, blue = LTO, green = binder and conductive additive. (For interpretation of the references to color in this figure legend, the reader is referred to the web version of this article.)

two sample holders and fixed with a polyacrylate double-sided adhesive tape (tesafix 5696, extra strong from Tesa SE). At the end of the test procedure, an analysis of the failure mode was perfomed. The failure mode (either adhesive or cohesive) was determined using the definition proposed by DIN EN ISO 4624 and DIN EN ISO 10,365. More details regarding the measurement method used can be found in [21]. The fractions of cohesive and adhesive breaking were calculated using an image-based MatLAB script.

Brunauer-Emmett-Teller (BET) surface area measurements were taken with a Quantachrome Monosorb rapid surface area analyser.

We calculated the roughness factor of the untreated and dendritic copper current collector in order to estimate the degree of physical surface enlargement by the following equations:

$$m_{\mathrm{Cu-sample}} = \frac{\rho_{\mathrm{Cu}}}{A_{\mathrm{geometric}} \cdot d_{\mathrm{Cu-foil}}} \tag{1}$$

$$A_{\mathrm{true}} = BET_{\mathrm{Cu-foil}} \cdot m_{\mathrm{Cu-sample}} = BET_{\mathrm{Cu-foil}} \cdot \frac{\rho_{\mathrm{Cu}}}{A_{\mathrm{geometric}} \cdot d_{\mathrm{Cu-sample}}} \tag{2}$$

$$RF = \frac{A_{\mathrm{true}}}{A_{\mathrm{geometric}}} = \frac{BET_{\mathrm{Cu-foil}} \cdot \rho_{\mathrm{Cu}}}{d_{\mathrm{Cu-sample}}} \tag{3}$$

A battery tester (CTS-LAB, BasyTec, Asselfingen, Germany) and a potentiostat (PGSTAT204, Metrohm, Fiderstadt, Germany) has been used for electrochemical characterization. Charge and discharge cycles were carried out with a constant current protocol between 1.0 V and 2.2 V. C-rates were calculated using the specific LTO capacity of 175 mAh/g, given by the supplier.

Formation was performed by applying two cycles at C/3. For subsequent EIS analysis along SOC, cells were first delithiated to 2.2 V at C/3 rate after formation. Hence, the cells were lithiated up to each point of investigation by applying C/3 rate for 30 min. Final EIS analysis was performed after reaching the lower voltage limit of 1.0 V. EIS measurements were carried out at 25 °C (INCU-Line IL 68 R, VWR, Ismanning, Germany) after 2 h rest at 0 V OCV, in the frequency range of 100 kHz – 10 mHz (potentiostatic mode) using 5 mV_{rms}. Equivalent circuit fit analysis of EIS data was performed using the Z-fit protocol within a MatLAB environment. EIS measurements were performed in three-electrode mode, where voltage was measured at the reference electrode and current at the counter electrode.

Measurement of internal resistance R_{AC} was performed as a measurement of IR-drop in a ten minute relaxation period between each charging and discharging step. R_{ac} describes the ohm part of the internal resistance and is calculated by the first measurement of the actual program step and the last measurement of the previous program step according to the following formula:

$$R_{ac} = \frac{\Delta U}{\Delta I} = \frac{U_2 - U_1}{I_2 - I_1} \tag{4}$$

To ensure reproducibility of the study, each test has been carried out in triplicate.

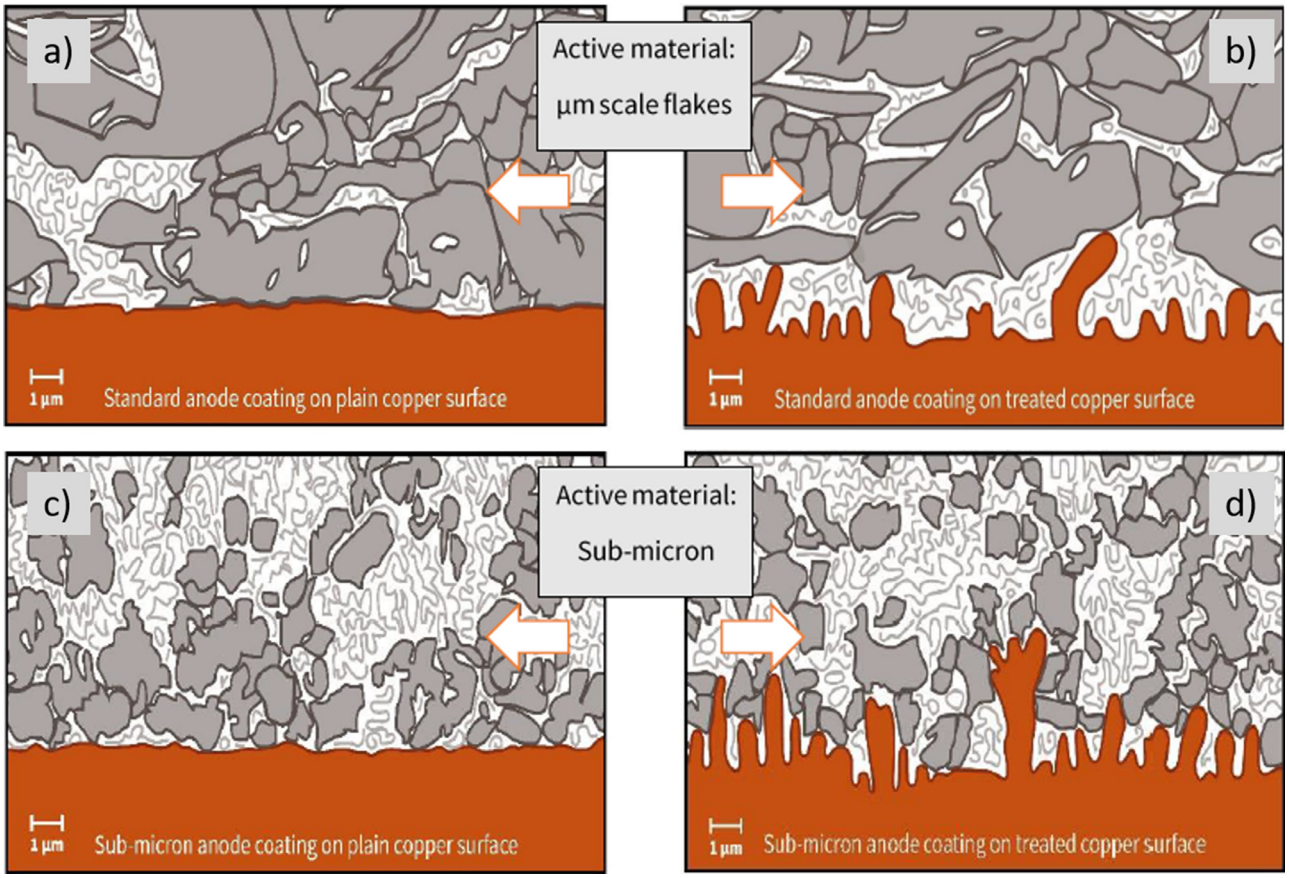

Fig. 3. Schematic illustration on connectivity of particles at different sizes; micrometre-scale flakes on plain (a) and treated (b) copper surface and sub-micron particles on plain (c) and treated (d) copper surface. Polymeric binder is pictured in light grey. (For interpretation of the references to color in this figure legend, the reader is referred to the web version of this article.)

3. Results and discussion

First results showed that platelet-shaped graphite with a particle size (D50) in the range of 22.8 µm is not the ideal material to be applied upon this type of galvanically structured current collector. This finding is mainly based on the fact that the nodule structure of the copper foil is taking place in a dimension of 200 nanometers which is clearly smaller than the particle size of 22.8 µm of the graphite. This fact is illustrated by Fig. 1. Therefore we have carried out experiments with (nano-sized) LTO as anode material with a particle size D90 below 10 µm.

The copper foils coated with the electrode slurry were examined by FIB/SEM and the obtained images are shown in Fig. 2. The untreated copper foil has a very smooth and clearly defined surface, whereas the modified foil shows distinct copper dendrites. A significantly improved connection between the LTO particles and dendritic copper foil is visible at first sight. The false colour image clearly confirms and illustrates this fact. It appears that the small LTO particles allow a higher amount of binder and carbon black to reach the treated foil and thereby enable some sort of mechanical anchoring. The particles marked in green represent binder and conductive additives and seem homogeneously dispersed within the composite electrode. The blue marked active material LTO is in good contact with binder/conductive additives and the copper collector foil.

To evaluate the effect of different morphology and dimensions, both active material flakes of graphite and nano-sized LTO were used and examined by FIB-SEM. Fig. 3 schematically shows how different particle sizes are able to connect with the treated copper foil. Obviously, the graphite active material in micrometre-range is too large to fit into the dendritic structure, and therefore mainly the binder attaches the copper surface - the over-sized active material can only reach the tips of the dendrites. Thus, no increased contact area between LTO particles and Cu foil is generated. Lowering the particle size of the active material down to sub-micron range results in highly improved contacts between both the active material and inactive materials like binder and conductive additives with the structured collector foil. Due to this improved contact, higher adhesion forces and a significantly reduced internal resistance should be reached.

BET measurement of dendritic copper foil resulted in a surface area of 0.03 m^2/g. The calculation of roughness factor with equations (1) - (3) ended up with the fact that the dendritic copper foil owns an 8-fold larger surface compared to the untreated foil (assumption: roughness factor of 1 in the case of uniformity).

Fig. 4a) compares the different failure mechanisms – adhesive breaking at the interphase between active material and current collector and cohesive breaking within the active material – for untreated and dendritic current collector. The fraction% values indicate the ratio between cohesive and adhesive breaking from all tested electrodes, evaluated according to DIN EN ISO 4624 and DIN EN ISO 10,365. It can be clearly seen that the degree of adhesive breaking is shifted to higher values for the dendritic current collector, meaning that a higher amount of adhesive breaking is taking place when using the dendritic one. Obviously, there is a disproportion between the particle size of the used LTO and the morphological structure of the dendritic current collector. Due to a lack of formation of a planar connection between the LTO particle

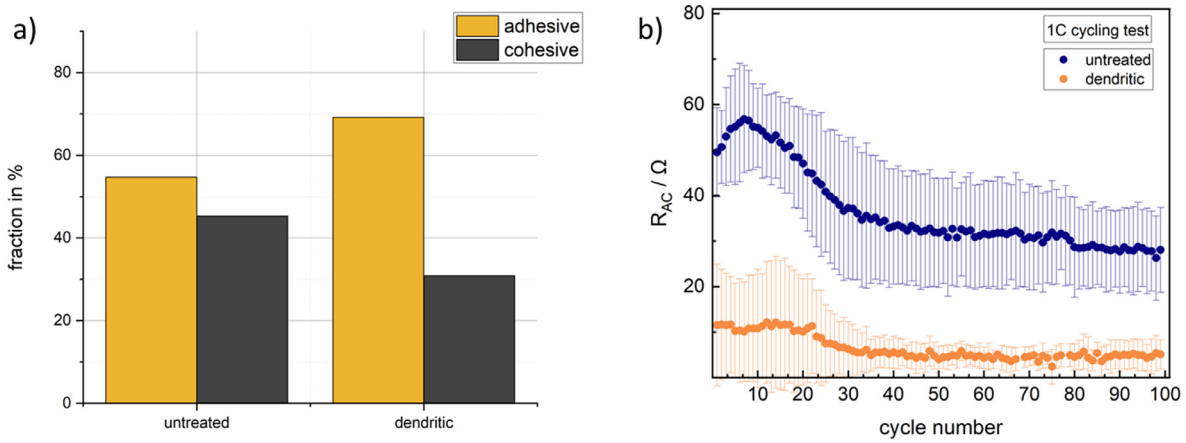

Fig. 4. Percentage of adhesive or cohesive failure mechanisms a) and internal resistance b) of LTO electrodes for untreated and dendritic copper foil as current collector.

and the current collector, the weakest point of the bonding joint is thus located at the edge between the coating and the Cu collector, which further leads to a higher percentage of adhesive failure for the dendritic current collector compared to the untreated situation. A possible solution to this problem would be to use the electrochemical benefit of the dendritic current collector by preparing a coating with even smaller LTO particles in order to enhance the interlocking of the LTO in the pores of the Cu foil. With a smaller LTO particle size, the stresses applied to the electrode can be more widely distributed at the interface between the electrode material and the current collector. This would enable more plastic energy dissipation to occur and lead to an increase in adhesion strength thus decreasing the percentage of adhesive failure. In order to exploit the real benefit of the surface foil preparation the size ratio between substrate pores and active material particle size should be considered.

Fig. 4b shows the internal resistance R_{AC} which is measured in-operando during cycling. This value is considerably reduced by a factor of 4.5 if comparing the LTO electrodes behaviour with untreated (blue) and galvanically structured (orange) copper foil. Although not as precise as EIS measurements, these values already indicate an enhanced interface of the dendritic copper foil in contrast to the untreated one. Concerning the phenomenon of increasing resistance, we assume a conditioning reaction of the copper surface – as the dendrites are owning a higher surface, the effect is not that visible in the case of the dendritic foil. This is verified by a significantly reduced spread width of the standard deviation. In contrast to the untreated foil, the dendritic one shows a clear stabilization of the interface and therefore its standard deviation is decreasing with increasing cycles. Furthermore, C-rate capability is clearly improved, which can be seen in Fig. 5, whereas an enlarged surface does not seem to show a significant difference for the ageing of electrodes during cycling test at 1C rate. A remarkable difference arises at application of highest C-rates above 5C. This corresponds to our original target, namely to improve electrode transition by increasing the interfacial area of LTO and copper foil.

T-cells consisting of a LTO working electrode, Li counter electrode and Li reference electrode were investigated in three-electrode-mode via EIS comparing their behaviour if untreated or dendritic copper current collectors were used along different states of charge. The EIS spectra were collected after three formation cycles (C/3 rate). Fig. 6 shows the respective impedance spectra.

The Nyquist plots show a distorted flat semicircle and the Warburg behaviour at the lowest frequencies. For data analysis, we used the equivalent circuit model shown in Fig. 7.

The equivalent circuit model shown in Fig. 7 was used for data analysis of the spectra in which two flat semicircles and a Warburg element is considered [22,23]. At the highest frequencies, ohmic resistance arises both from electrolyte and environment setup. Surface resistance phenomena are represented by the first semicircle, while the second semicircle arises from the LTO charge transfer reaction. LTO is usually considered to form negligible passivation layers [24,25] due to its relatively high potential, therefore main influence on the surface resistance should come from the electrode current collector interface . Solid state diffusion phenomena are responsible for low frequency response [26]. While the resistance contribution due to SEI layer remains constant and independent from the SOC, the contribution related to the charge transfer increase with SOC. For some other active materials like NMC and graphite a similar SOC-dependency was already found; the charge-transfer signal of graphite [2] and NMC [27] decreases with increasing SOC. Due to the fact that the charge-transfer signal represents an intrinsic material parameter, a comparison between different materials might be questionable. Other groups have evaluated quite similar fitting parameters and a likewise impedance signal for LTO-based electrodes [7,22]

In Fig. 6 the data point at 1 kHz (cyan highlighted) is close to the end of the semicircle in all the plots and its relative position seems not be affected by SOC for any of the cells. First, this behaviour clearly excludes any changes in the system time constant throughout the measurements and secondly, $R_{surface}$ originating the first semicircle can be regarded as independent from SOC. Fig. 8 shows the results from the data fitting in which the Warburg behaviour was excluded.

The values of Q_{CT}, i.e. the double layer capacitance in parallel with the charge transfer resistance, lie around 10 – 30 $\mu F \bullet s^{(a-1)} \bullet cm^{-2}_{geo}$ for all cells with negligible dependence on SOC. $Q_{surface}$ values show no significant correlation to the SOC and lie around 6 – 13 $\mu F \bullet s^{(a-1)} \bullet cm^{-2}_{geo}$ for cells coated on untreated copper current collector, while LTO electrodes coated on dendritic current collector reveal significantly increased capacitance fit parameters around 17 – 43 $\mu F \bullet s^{(a-1)} \bullet cm^{-2}_{geo}$. Similarly, the surface resistance fit parameters have no significant correlation to SOC for any cell, though the introduction of a dendritic current collector in LTO electrodes significantly lowers the surface resistance fit parameters from 27 – 34 $\Omega \bullet cm^2_{geo}$ to 4 – 15 $\Omega \bullet cm^2_{geo}$.

Differently than surface resistance, the LTO charge-transfer resistances increase linearly with SOC for all cells. Both phenomena do not indicate any dependence on the copper current collector geometry. It is more likely for the charge-transfer resistance to depend on the used electrolyte, as discussed by De Giorgio et al. [7]. Ma et al. showed comparable impedance parameters for a compa-

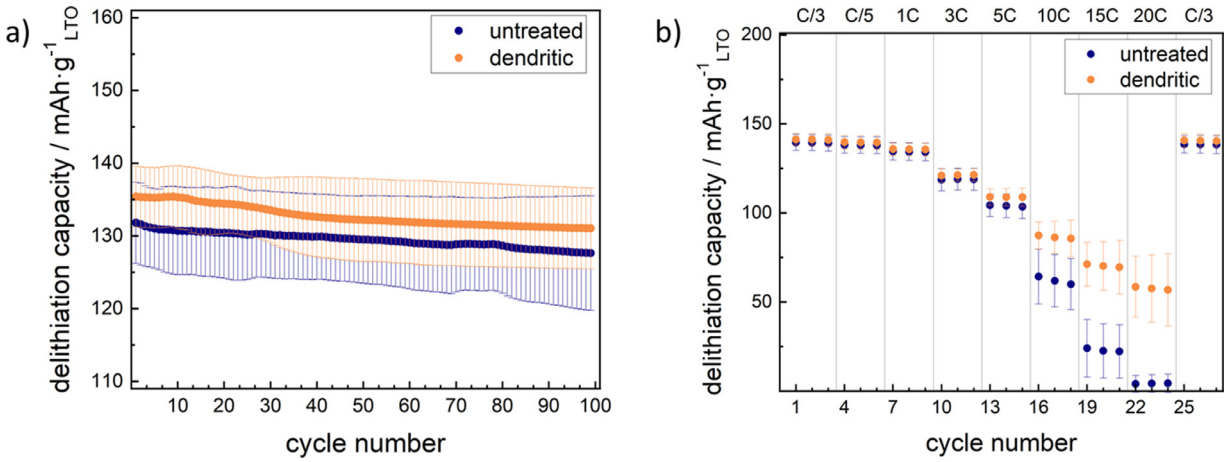

Fig. 5. Galvanostatic charge/discharge test a) and C-rate test b) of LTO electrodes with untreated and dendritic current collector. The error bars are also displayed.

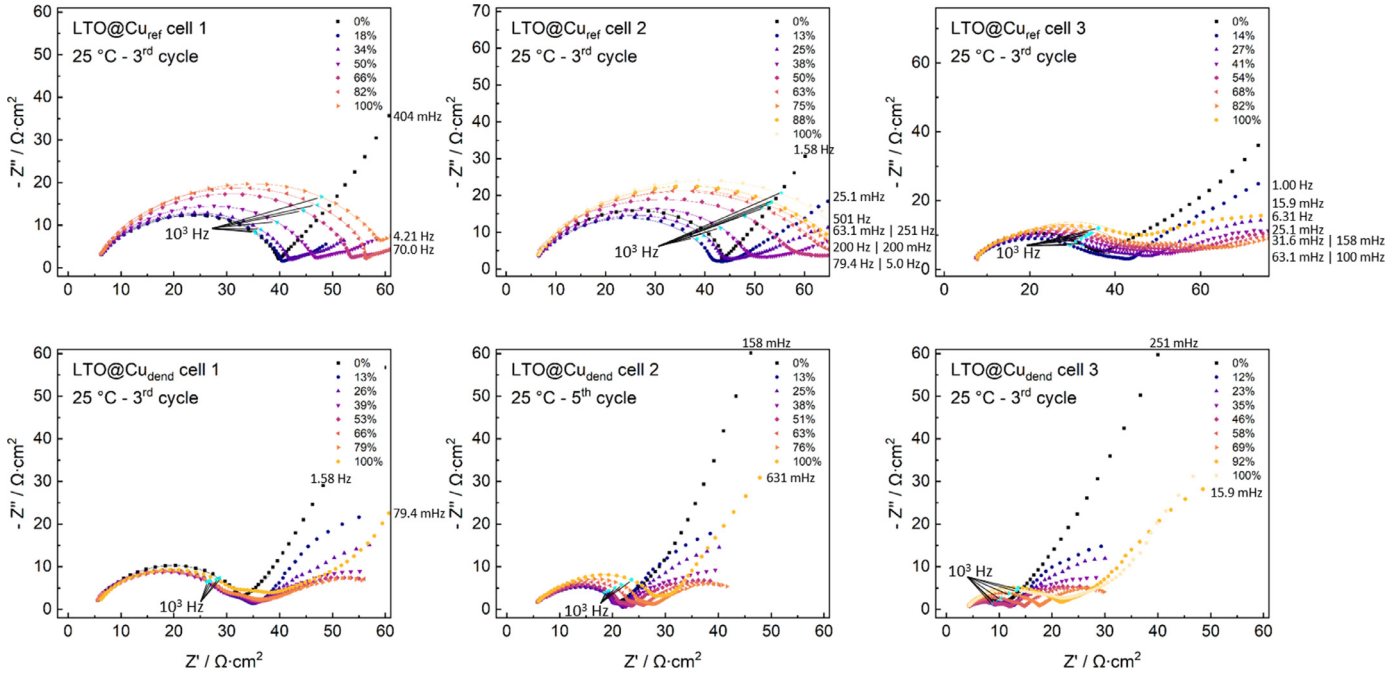

Fig. 6. Impedance measurements (100 kHz – 10 mHz) of LTO electrodes on untreated or dendritic current collectors; three-electrode (T-cell) geometry; fitting curves indicated as solid lines; the data points at 1 kHz highlighted in pale blue; frequencies of final datapoints indicated for partially visible datasets. 10^3 Hz indication as tracer for EIS time constant shifts. (For interpretation of the references to color in this figure legend, the reader is referred to the web version of this article.)

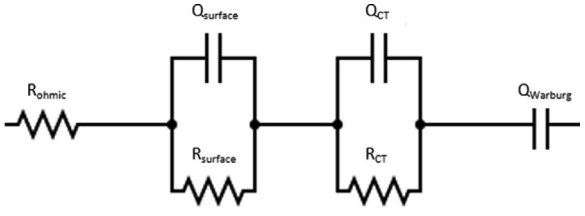

Fig. 7. Equivalent circuit model used for EIS fit analysis.

rable electrolyte, but a different dependency on SOC [22] probably due to the different particle size. Kawade et al. though focusing on connection resistance of nanoparticles, reported in a similar order of magnitude for charge-transfer resistance [23]. Our fit parameters are also supported by several further publications with charge-transfer resistance values in likewise dimensions [2,24,25]

The decrease of the surface fit parameter of the electrode with dendritic current collector indicates a normalization discrepancy. While all fit parameters were normalized to the geometric electrode area, all surface resistance signals should truly depend on the electrochemically active interface area A_{true}. So obviously, the fitting parameters can be used as a measure for the electrochemically active interface area between LTO and copper foil. Further evaluation requires a statistical analysis of the respective fit parameters, which is shown in Fig. 9.

The analysis of the generated EIS fit parameters provides two independent signal shifts, one for $R_{surface}$ and one for $Q_{surface}$, bound to the difference in true electrochemically active interface. The normalization shift factor $f_{normalization}$ results from the ratio between $A_{active\text{-}dendritic}$ and $A_{active\text{-}reference}$, where $A_{active\text{-}dendritic}$ and $A_{active\text{-}reference}$ are the fit values at each SOC of $R_{surface}$ and $Q_{surface}$ reported in Fig. 9.

$$f_{normalization\ shift}\ [A_{active}] = \frac{A_{active-dendritic}}{A_{active-reference}} \quad (5)$$

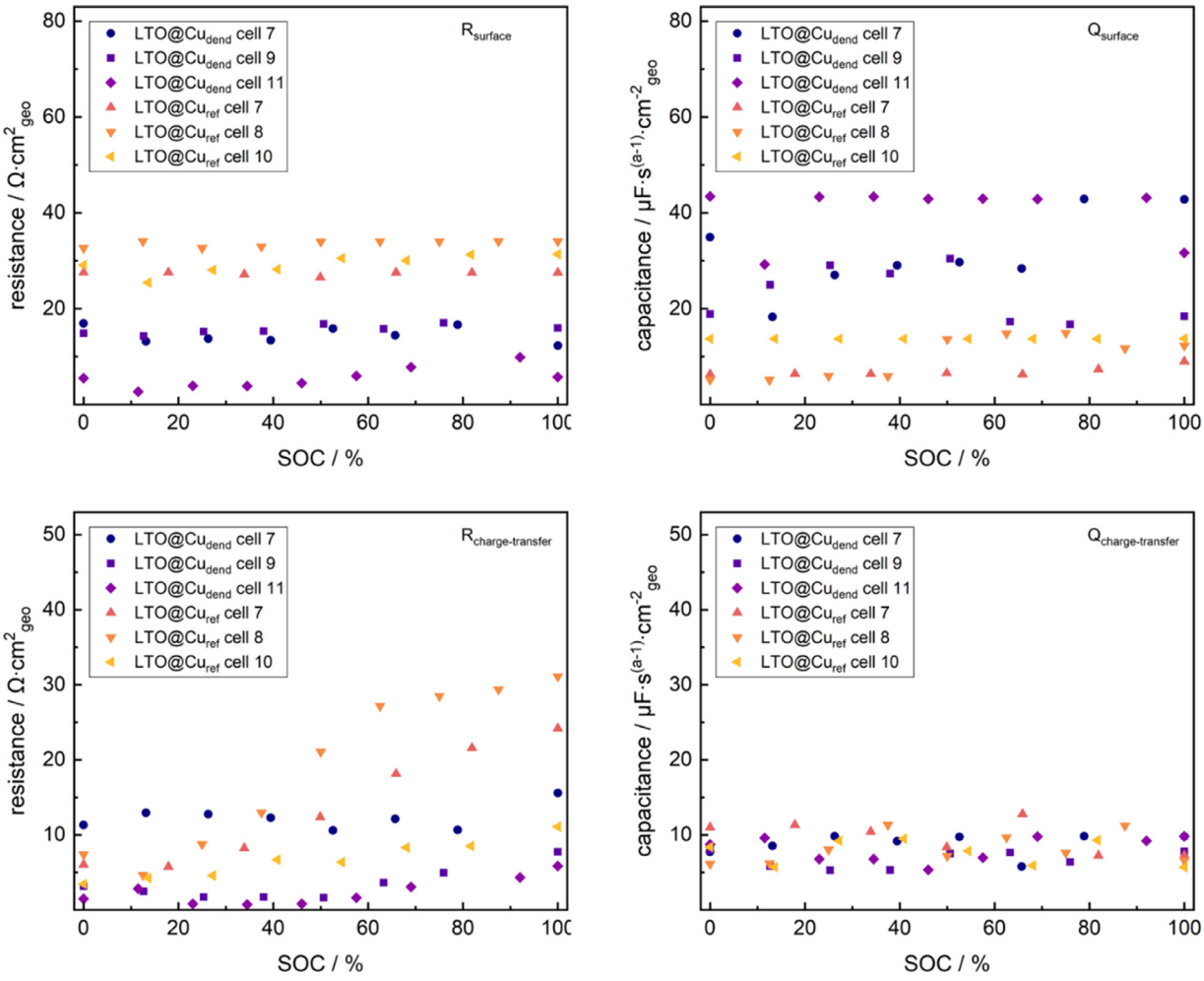

Fig. 8. EIS fitting parameters of LTO electrodes with untreated or dendritic current collectors, along 3rd cycle lithiation step; data normalized to geometric electrode area.

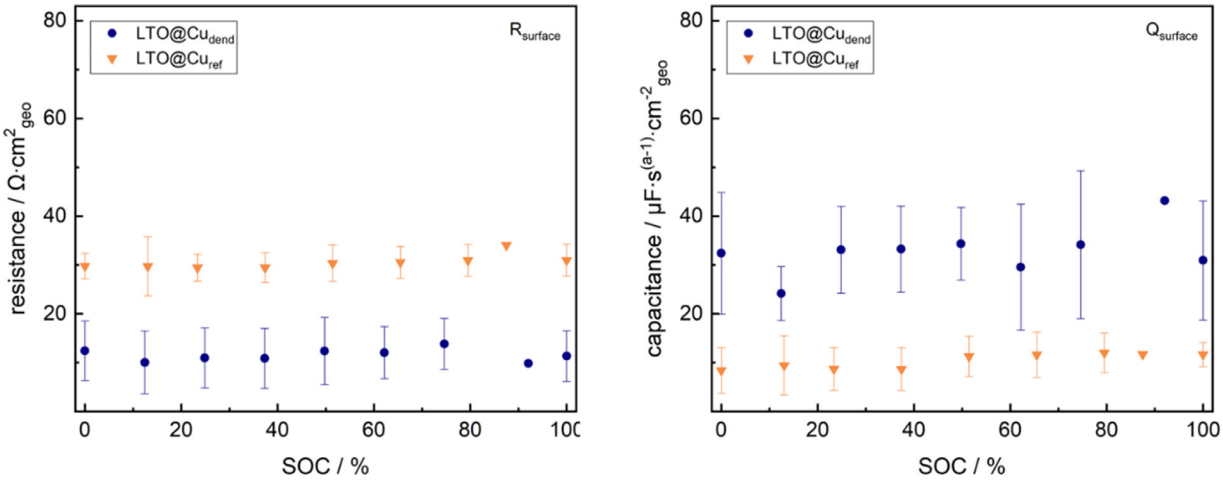

Fig. 9. Averaged EIS fitting parameters of LTO electrodes with untreated or dendritic current collectors, along 3rd cycle lithiation step; data normalized to geometric electrode area. The point near 90% is the result of a single measurement.

This normalization shift factor $f_{normalization\ shift}$ for electrochemically active interface area is also capable to compare the physical surface areas of dendritic and untreated copper foil by indicating a roughness factor RF.

$$f_{normalization\ shift}\ [A_{true}] = \frac{A_{true-dendritic}}{A_{true-reference}} = \frac{RF_{dendritic}}{RF_{reference}} \quad (6)$$

So finally, $f_{normalization\ shift}$ allows for a direct comparison of electrochemically active interface area shift and physical surface increase, between dendritic and reference copper foil. This is visualized in Fig. 10.

While the physical surface increase in interface area, given by the roughness factor shift, lies at ≈ 7.9, an electrochemically active shift of ≈ 3.8 or ≈ 3.3 is found for the surface capacitance shift

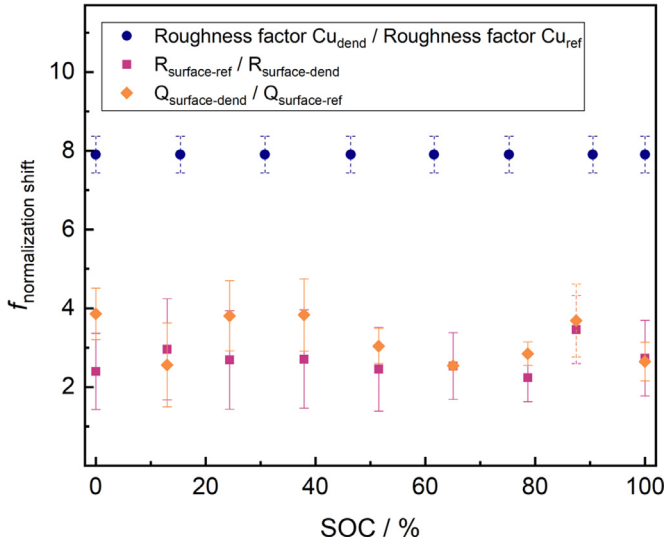

Fig. 10. Comparison of surface increase factors at the electrode-current collector interface, determined via roughness factor shift, surface capacitance shift and surface resistance shift; measured error bars indicated as solid lines, estimated error bars indicated as dashed lines. (For interpretation of the references to color in this figure legend, the reader is referred to the web version of this article.)

Table 1
Averaged EIS fit parameters of LTO electrodes.

material	surface capacitance [$\mu F \bullet s^{(a-1)} \bullet cm^{-2}{}_{geo}$]	surface resistance [$\Omega \bullet cm^2{}_{geo}$]
$LTO@Cu_{dendritic}$	25 ± 7	15 ± 6
$LTO@Cu_{reference}$	8 ± 3	39 ± 4

and surface resistance shift, respectively. Consequently, 32 – 45% of the increased surface area of the dendritic current collector are electrochemically active in the designed system.

Conclusions

We successfully prepared LTO anodes for the use in lithium-ion batteries on dendritic copper current collectors. Evaluation of the surface modification was performed via mechanical analysis, FIB-SEM and electrochemical measurements. The investigations verified the existence of distinct copper dendrites leading to a physically increased surface area of the current collector. Differences in terms of inner resistance, rate capability at high current and surface resistance confirmed a clear difference in active area between untreated and dendritic current collectors due to the modified surface. Furthermore, a higher capacitance and a lowered surface resistance were found for the electrodes with the dendritic current collector in contrast to the ones with the copper reference. This indicates an improved connection between the current collector and the anode material, thus also proving an increase in electrochemically active surface area. Based on these findings, further research will be carried out to gain new insights into structural improvements for an enhanced performance of LTO anodes.

Fig. 1, Table 1

Credit author statement

Christina Toigo: methodology, writing – original draft, conceptualization, resources, data curation, visualization, project administration, funding acquisition

Martin Frankenberger: methodology, conceptualization, data curation, funding acquisition, writing – review and editing, visualization

Nicolas Billot: Investigation, writing – review and editing

Claudia Pscherer: Investigation

Benedikt Stumper: writing – review and editing

Fabian Distelrath: investigation, writing – review and editing, resources

Jonathan Schubert: investigation, writing – review and editing

Karl-Heinz Pettinger: validation, writing – review and editing, supervision

Catia Arbizzani: validation, writing – review and editing, supervision

Declaration of Competing Interest

The authors declare that they have no known competing financial interests or personal relationships that could have appeared to influence the work reported in this paper.

Acknowledgments

The authors thank for financial support by Erasmus+ program, grant number 2019-1-IT02-KA103-061398 and BMWi (Federal Ministry for Economic Affairs and Energy, Germany), grant number 03ET6103C and BlueSky Energy GmbH.

Supplementary materials

Supplementary material associated with this article can be found, in the online version, at doi:10.1016/j.electacta.2021.138978.

References

[1] Martin Frankenberger, Madhav Singh, Alexander Dinter, Sebastian Jankowksy, Alexander Schmidt, Karl-Heinz Pettinger, Laminated Lithium Ion Batteries with improved fast charging capability, Journal of Electroanalytical Chemistry 837 (2019) 151–158.
[2] Martin Frankenberger, Madhav Singh, Alexander Dinter, Karl-Heinz Pettinger, EIS Study on the Electrode-Separator Interface Lamination, Batteries 5 (2019) 71.
[3] Christina Toigo, Madhav Singh, Benjamin Gmeiner, Maurizio Biso, Karl-Heinz Pettinger, A Method to Measure the Swelling of Water-Soluble PVDF Binder System and Its Electrochemical Performance for Lithium Ion Batteries, Journal of The Electrochemical Society 167 (2020) 20514.
[4] Christina Toigo, Catia Arbizzani, Karl-Heinz Pettinger, Maurizio Biso, Study on Different Water-Based Binders for Li4Ti5O12 Electrodes, Molecules (Basel, Switzerland) 25 (2020) 2443.
[5] Diogo Vieira Carvalho, Nicholas Loeffler, Guk-Tae Kim, Mario Marinaro, Margret Wohlfahrt-Mehrens, Stefano Passerini, Study of Water-Based Lithium Titanate Electrode Processing: The Role of pH and Binder Molecular Structure, Polymers 8 (2016) 276.
[6] V.V.N. Phanikumar, Vallabha Rao Rikka, Bijoy Das, Raghavan Gopalan, B V.Appa Rao, Raju Prakash, Investigation on polyvinyl alcohol and sodium alginate as aqeuous binders for lithium-titanium oxide anode in lithium-ion batteries, Ionics 25 (2019) 2549–2561.
[7] Francesca De Giorgio, Andrea La Monaca, Alexander Dinter, Martin Frankenberger, Karl-Heinz Pettinger, Catia Arbizzani, Water-processable Li4Ti5O12 electrodes featuring eco-friendly sodium alginate binder, Electrochimica Acta 289 (2018) 112–119.
[8] Agnese Birrozzi, Mark Copley, Jan von Zamory, Marta Pasqualini, Silvia Calcaterra, Francesco Nobili, Andrea Di Cicco, Hanna Rajantie, Martha Briceno, Edward Bilbé, Laura Cabo-Fernandez, Laurence J. Hardwick, Dominic Bresser, Stefano Passerini, Scaling up "Nano" Li 4 Ti 5 O 12 for High-Power Lithium-Ion Anodes Using Large Scale Flame Spray Pyrolysis, Journal of The Electrochemical Society 162 (2015) A2331–A2338.
[9] Saravanan Karuppiah, Sylvian Franger, Kalaiselvi Nallathamby, Water-soluble green binder for Li4Ti5O12 anodes: Effect of binder choice on Lithium Storage, ChemElectroChem 5 (2018) 343–349.
[10] Binh Tran, Isaiah O. Oladeji, Zedong Wang, Jean Calderon, Guangyu Chai, David Atherton, Lei Zhai, Adhesive PEG-based binder for aqueous fabrication of thick LTO electrode, Electrochimica Acta 88 (2013) 536–542.
[11] So-Jin; Kim, Bo-Ram; Lee, Eun-Suok Oh, Application of a bio-derivative, rosin, as a binder additive for lithium titanium oxide electrodes in lithium-ion batteries, Journal of Power Sources 273 (2015) 608–612.
[12] Jiangmin Jiang, Ping Nie, Bing Ding, Wenxin Wu, Zhi Chang, Yuting Wu, Hui Dou, Xiaogang Zhang, Effect of Graphene Modified Cu Current Collector on the Performance of Li4Ti5O12 Anode for Lithium-Ion Batteries, ACS applied materials & interfaces 8 (2016) 30926–30932.

[13] Hsien-Chang Wu, Yen-Po Lin, Eric Lee, Wen-Ting Lin, Jui-Kai Hu, Hung-Chang Chen, Nae-Lih Wu, High-performance carbon-based supercapacitors using Al current-collector with conformal carbon coating, Materials Chemistry and Physics 117 (2009) 294–300.
[14] Ningxin Zhang, Yijing Zheng, Atanaska Trifonova, Wilhelm Pfleging, Laser structured Cu foil for high-performance lithium-ion battery anodes, Journal of Applied Electrochemistry 47 (2017) 829–837.
[15] Wilhelm Pfleging, Melanie Mangang, Yijing Zheng, Peter Smyrek, Laser structuring for improved battery performance, SPIE Newsroom (2016).
[16] Shuwen Kang, Haiming Xie, Wei Zhai, Zi-feng Ma, Rongshu Wang, Weimin Zhang, Enhancing performance of a Lithium Ion Battery by Optimizing the Surface Properties of the Current Collector, International Journal of Electrochemical Science 10 (2015) 2324–2335.
[17] Tatsuya Nakamura, Shingo Okano, Noriko Yaguma, Yukari Morinaga, Hikari Takahara, Yoshihiro Yamada, Electrochemical performance of cathodes prepared on current collector with different surface morphologies, Journal of Power Sources 244 (2013) 532–537.
[18] Yijing Zheng, Z. An, Peter Smyrek, Hans Jürgen Seifert, Wilhelm Pfleging, Tim Kunze, Valentin Lang, Andrés Lasagni, Laser interference patterning and laser-induced periodic surface structure formation on metallic substrates, in: 2016 IEEE International Conference on Manipulation, Manufacturing and Measurement on the Nanoscale (3M-NANO), 2016, IEEE, 2016, pp. 159–163.
[19] Jan B. Habedank, Ludwig Kraft, Alexander; Rheinfeld, Christina; Krezdorn, Andreas; Jossen, Michael F. Zaeh, Increasing the Discharge Rate Capability of Lithium-Ion Cells with Laser-Structured Graphite Anodes: Modeling and Simulation, Journal of The Electrochemical Society 165 (2018) A1563–A1573.
[20] Robert Morasch, Johannes Landesfeind, Bharatkumar Suthar, Hubert A. Gasteiger, Detection of Binder Gradients Using Impedance Spectroscopy and Their Influence on the Tortuosity of Li-Ion Battery Graphite Electrodes, Journal of The Electrochemical Society 165 (Nr. 14) (2018) A3459–A3467.
[21] Nicolas Billot, Till Günther, David Schreiner, Ralf Stahl, Jakob Kranner, Moritz Beyer, Gunther Reinhart, Investigation of the Adhesion Strength along the Electrode Manufacturing Process for Improved Lithium-Ion Anodes, Energy Technology 8 (2020) 1801136.
[22] Miaomiao Ma, Azzam N. Mansour, Jonathan K. Ko, Gordon H. Waller, Christopher E. Hendricks, Characterization of Li Diffusion and Solid Electrolyte Interface for Li 4 Ti 5 O 12 Electrode Cycled with an Organosilicon Additive Electrolyte, Journal of The Electrochemical Society 167 (2020) 110549.
[23] Ujjwala V. Kawade, Manish S. Jayswal, Anuradha A. Ambalkar, Sunil R. Kadam, Rajendra P. Panmand, Jalinder D. Ambekar, Milind V. Kulkarni, Bharat B. Kale, Surface modified Li 4 Ti 5 O 12 by paper templated approach for enhanced interfacial Li + charge transfer in Li-ion batteries, RSC Advances 8 (2018) 38391–38399.
[24] Miran Gaberscek, Joze Moskon, Bostjan Erjavec, Robert Dominko, Janez Jamnik, The Importance of Interphase Contacts in Li Ion Electrodes: The Meaning of the High-Frequency Impedance Arc, Electrochemical and Solid-State Letters 11 (2008) A170.
[25] Yuya Ishihara, Kohei Miyazaki, Tomokazu Fukutsuka, Takeshi Abe, Kinetics of Lithium-Ion Transfer at the Interface between Li4Ti5O12 Thin Films and Organic Electrolytes, ECS Electrochemistry Letters 3 (2014) A83–A86.
[26] Andreas Jossen, Wolfgang Weydanz, Moderne Akkumulatoren richtig einsetzen. 2. überarbeitete Auflage, Cuvillier Verlag, Göttingen, 2019.
[27] Wladislaw Waag, Stefan Käbitz, Dirk Uwe Sauer, Experimental investigation of the lithium-ion battery impedance characteristic at various conditions and aging states and its influence on the application, Applied Energy 102 (2013) 885–897.